ADVANCED MATERIALS

High-Performance Organic Single-Crystal Transistors on Flexible Substrates**

By *Alejandro L. Briseno, Ricky J. Tseng, Mang-Mang Ling, Eduardo H. L. Falcao, Yang Yang,* *Fred Wudl,* and *Zhenan Bao**

The electronic properties of organic single crystals have been intensely studied for well over 40 years.[1,2] Until recently, organic single-crystal field-effect transistors have generated results that are comparable to and sometimes better in performance than hydrogenated amorphous silicon.[3–11] Organic thin-film transistors are being actively pursued for a broad area of electronic applications, but their charge-carrier mobilities are limited by structural imperfections (i.e., grain boundaries) and impurities. Organic single crystals, on the other hand, have been limited to charge-transport studies mainly because the fabrication of single-crystal transistors poses a technological challenge. Novel methods for fabricating single-crystal devices include the flip-crystal technique,[3] elastomeric stamp platforms,[4–6] and freestanding devices,[7–10] where the source–drain electrodes, dielectric, and gate are all fabricated onto the crystal surface. For the most part, a relatively thick and rigid single crystal is employed (5–500 μm thick). Because the fragility makes them difficult to handle, their use has been restricted to simple and basic devices and wide-ranging applications in sensors or plastic transistors for flexible electronics have not yet been possible. Thus, there is a strong need for the development of mechanically flexible, nondestructive, single-crystal devices with prospective applications in organic electronics while maintaining the intrinsic properties and characteristics of organic single crystals.

We demonstrate field-effect transistors fabricated from thin and conformable organic single crystals. We report on proof-of-concept "flexible" organic single-crystal field-effect transistors with performance exceeding those of previously reported organic thin-film flexible devices.[12] Rubrene single-crystal devices constructed on low-cost flexible substrates (Fig. 1b) yielded mobilities as high as 4.6 cm^2 V^{-1} s^{-1} and on/off ratios of approximately 10^6.
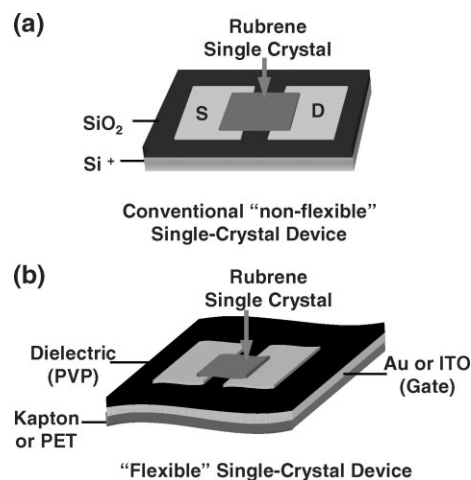
Figure 1. Bottom-contact single-crystal device configuration. Lithographically prepared gold source–drain electrodes were used for a) conventional rigid devices and b) shadow-mask-prepared source–drain electrodes for flexible single-crystal devices. Au–Kapton and/or transparent indium tin oxide (ITO)–PET (PET: poly(ethylene terephthalate) substrates were used for bottom-contact flexible substrates. PVP: poly-4-vinylphenol.

[*] Prof. Y. Yang, R. J. Tseng
Department of Materials Science and Engineering
University of California
Los Angeles, CA 90095 (USA)
E-mail: yangy@ucla.edu

Prof. Z. Bao, Dr. M.-M. Ling
Department of Chemical Engineering
Stanford University
Stanford, CA 94305 (USA)
E-mail: zbao@chemeng.stanford.edu

A. L. Briseno, Dr. E. H. L. Falcao, Prof. F. Wudl
Department of Chemistry and Biochemistry and
Exotic Materials Institute
University of California
Los Angeles, CA 90095 (USA)

Our fabrication technique begins with the growth of single crystals by physical vapor transport in a flowing stream of argon.[13] Rapid growth conditions enabled single crystals to grow as thin as 150 nm and as large as 1 cm × 1 cm in size (see Experimental). We note that our thin crystals are at least 300 times thinner than typical crystals used to fabricate single-crystal transistors. Rubrene single crystals were grown from commercially available material (Aldrich). Other than a standard vacuum sublimation and the physical vapor transport process of growing the crystals, no further efforts were made to purify the material. The quality of the single crystals was confirmed from the large birefringence observed under cross-

polarized light and from the narrow peak with a full width at half maximum of 0.02° corresponding to the (002) Bragg diffraction. The gold source–drain electrodes supporting thin rubrene single crystals on bottom-contact devices with SiO_2 dielectrics (Fig. 1a) were modified with a self-assembled-monolayer: 4-nitrobenzenethiol (NB). It has been well-documented[14,15] that source–drain electrodes modified with NB improve charge injection by increasing the carrier density near the contact metal/organic active layer interface. We note, however, that flexible rubrene devices were not modified with NB. For conventional devices, thin single crystals were electrostatically bonded against a doped Si/SiO_2 (300 nm) substrate with lithographically defined bottom-contact source–drain electrodes, while for flexible devices, the thin crystals were electrostatically adhered onto bottom-contact source–drain electrodes (evaporated through a shadow mask) with a poly-4-vinylphenol (PVP) thin film serving as the dielectric layer (Fig. 1b). All measurements on single-crystal devices were made in a normal room atmosphere.

Our investigation of organic single crystals begins by first examining the performance of thin, single crystals electrostatically laminated onto conventional rigid substrates (i.e., Si/SiO_2). We then extend the study of "flexible" single crystals onto mechanically bendable substrates. This proof-of-concept study potentially makes it possible to use organic single crystals for a broader range of 'flexible applications' that have been previously dominated by inorganic,[16] solution-processed[17] SWNTs,[18] and polycrystalline organic semiconductor[12,19] transistors. Rubrene single crystals ranging from 150 nm to ~25 μm in thickness were confirmed by using atomic force microscopy (AFM), scanning electron microscopy (SEM), and profilometry. Figure 2a shows the electrical characteristics of a conventional transistor containing a thin,

electrostatically bonded rubrene single crystal. The output characteristics for a rubrene single-crystal device show well-resolved saturation currents for several values of gate voltage, while Figure 2b shows a plot of both the log and the square-root of drain current as a function of gate voltage. We extract a field-effect mobility of 2.6 cm^2 V^{-1} s^{-1} in the saturation region, on/off ratios greater than 10^4, a switch-on voltage of –11 V, and a normalized subthreshold swing, S, of 4.5 V nF decade^{-1} cm^{-2} at a drain–source voltage, V_{DS} = –100 V (see Table 1). Here, we report the field-effect onset as "normalized subthreshold swing" for the convenience of comparing our de-

Table 1. Summary of the electrical characteristics of rubrene single-crystal devices fabricated from non-flexible and flexible devices.

Device	Mobility [cm^2/V·s]	On/Off	V_T [V]	S [V·nF/decade·cm^2]
Non-flexible rubrene device	2.6	1.28×10^4	–11	4.5
Flexible rubrene device	4.6	~10^6	–2.1	0.9

vice characteristics with other reported devices.[7,11] From Figure 2c, the device characteristics reveal that single-crystal devices show little or no gate dependence beyond –20 V when mobility is plotted versus the gate voltage from the equation given by $\mu = (2 L/W C_i)(\partial I_{DS}^{1/2}/\partial V_G)^2$ (variables are as defined in the caption of Fig. 2).[20] Therefore, our electrostatically bonded single-crystal devices show gate-voltage-independent carrier mobility, which may clearly indicate that gate-voltage dependence is a more prevalent phenomenon commonly observed with interfacial defects or grain boundaries found in polycrystalline thin films.[21]

A close analysis of the thin, conformable single crystals shows a nearly defect-free surface morphology. Figure 3a and b show AFM images of the surface morphology of thin and thick rubrene single crystals, respectively. We find that thin single crystals (i.e., 150 nm–1 μm) have smaller and less frequent surface steps compared to thicker crystals. A surface scan over a 2 μm × 2 μm area at random locations on different individual samples yielded only one surface step (Fig. 3a). The surface roughness of a 300 nm thin rubrene single crystal is 0.23 nm, indicating a rather flat surface. A surface island is observed with a monolayer step height of approximately 15 Å, as shown in the inset, consistent with reported observations.[5,8] However, a scan of thicker crystals (>3 μm)
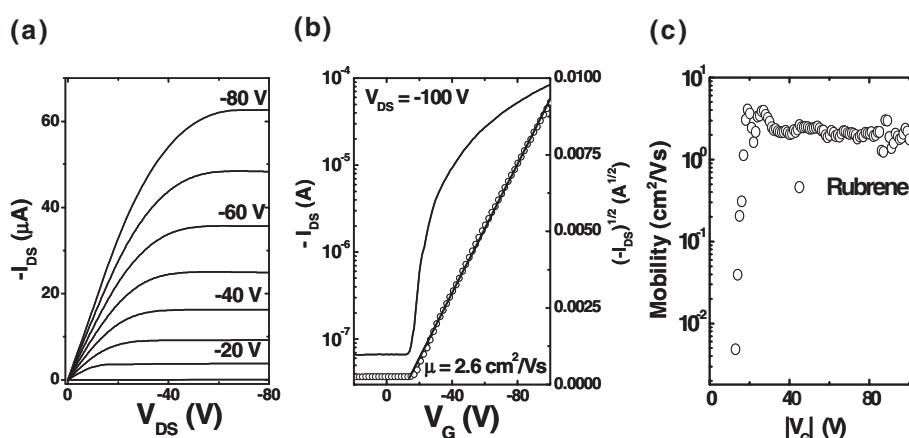

Figure 2. Electrical characteristics of conventional rubrene non-flexible devices. a) Electrical-output characteristics (channel width, W = 400 μm, channel length, L = 350 μm) and b) corresponding transfer and $I_{DS}^{1/2}$–V_G curve. Saturation-regime mobilities were calculated by the given equation, $I_{DS} = (W C_i \mu / 2 L)(V_G - V_T)^2$ (V_{DS} = –100 V). c) A plot of mobility versus gate voltage for a rubrene single-crystal device. The data were calculated from the given equation, $\mu = (2 L/W C_i)(\partial I_{DS}^{1/2}/\partial V_G)^2$. I_{DS}: drain–source current; V_G: gate voltage; μ: mobility; V_T: treshold voltage V_{DS}: drain–source voltage; C_i: capacitance of the dielectric.

(a) **(b)** **(c)**
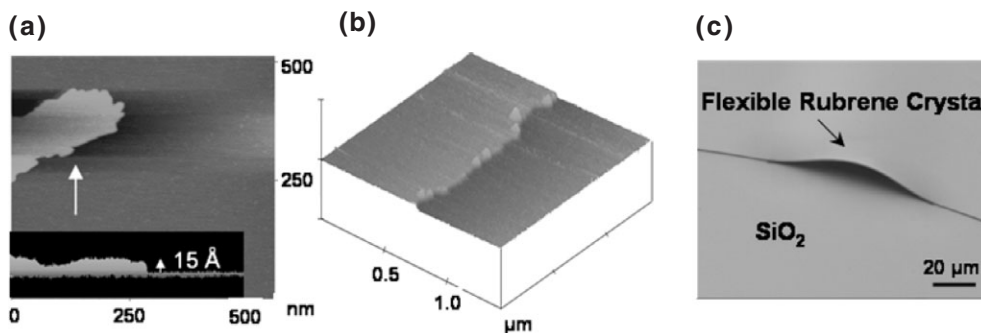
Figure 3. Surface analysis of rubrene single crystals. a) AFM image of an approximately 300 nm thin rubrene crystal (inset shows a topological side view in the direction from the indicated arrow) and b) a thicker rubrene crystal (> 3 μm). Larger and more frequent surface steps can be observed in thicker crystals. c) An SEM image of a thin (~ 1 μm) rubrene single crystal electrostatically adhered to a substrate. The curved crystal shows no interfacial or surface damage even after acute bending. Single crystals thicker than 3 μm tend to shatter or break when they are bent or curved.

showed more frequent and much larger surface steps (Fig. 3b) with a surface roughness of at least twice that of thin crystals. A higher degree of interfacial adhesion and surface conformity is observed with thin crystals compared to thicker crystals. Figure 3c shows an SEM image of a curved rubrene single crystal electrostatically adhered to a substrate. No noticeable damage to the crystal occurred even after severe bending. We conducted field-effect experiments to monitor the effective mobility at various crystal thicknesses. Results from Figure 4a show that mobility gradually drops as a function of crystal thickness. For thick crystals, greater than 5 μm, the mobility is less than 10^{-1} $cm^2 V^{-1} s^{-1}$ which we attribute to poor conformability and poorer interfacial contacts to the dielectric interface than the flexible and thin crystals. However, we are not suggesting that the quality of the crystal diminishes as the thickness increases, but rather we believe that thin crystals tend to conform to substrates more easily. Figure 4b shows a comparison of thin, nearly transparent rubrene single crystals and standard thick crystals (≫ 3 μm). The inset illustrates the natural flexibility of a thin rubrene single crystal as it bends on the tip of a tweezer.

We further extend our analysis of thin and conformable single crystals onto mechanically flexible substrates to yield conceptual devices that illustrate potential use in practical flexible electronics. Figure 5a and b show the output and transfer characteristics of a rubrene flexible transistor. Typical output $V_{DS} - I_{DS}$ curves show up to 280 μA at a gate voltage of only –60 V. A mobility of 4.6 $cm^2 V^{-1} s^{-1}$, on/off ratio of approximately 10^6, switch-on voltage of –2.1 V, and a normalized subthreshold swing of 0.9 V nF $decade^{-1} cm^{-2}$ is generated from a device fabricated on low-cost flexible substrates. Figure 5c shows a digital image of a typical rubrene transistor fabricated on a transparent and flexible poly(ethylene terephthalate) (PET) substrate (see Fig. 1b for configuration). It should also be noted that all single-crystal transistors examined in this study (both on conventional and flexible substrates) follow the square law, and the fitting line used for calculating mobility fits the data over a wide range of V_G values (Figs. 2b and 5b). We caution that mobilities reported here do not consider

(a)

(b)
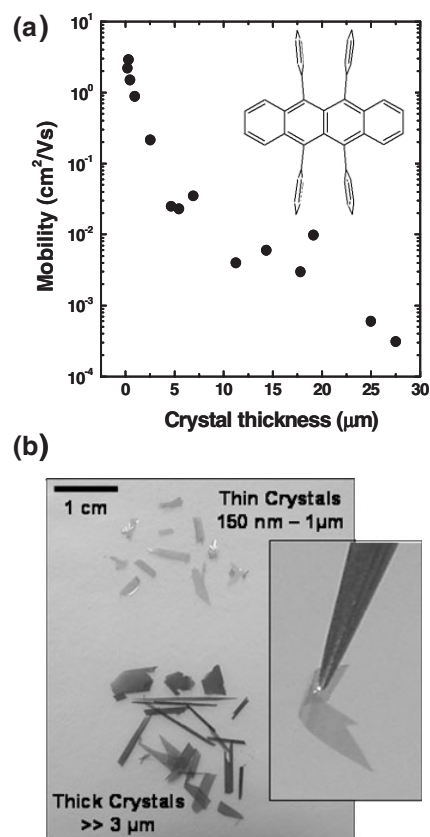
Figure 4. Charge-carrier mobility of rubrene single-crystal transistors plotted as a function of crystal thickness. a) The plot shows the decrease in measured mobility as crystal thickness increases (0.2–27 μm). b) Digital photograph comparing thin and thick rubrene single crystals. Thinner crystals are nearly transparent and flexible as captured from the inset that illustrates a thin crystal naturally "bending" at the tip of a tweezer. This particular attribute enables the high-quality single crystals to conform to curvaceous substrates thus allowing bending experiments to be conducted. The thicker rubrene crystals (dark grey in color) are not capable of mechanical bending and as a result of their fragility, applications have been mostly limited to charge-transport studies. Both crystals are grown from the same starting material, but under different growth conditions.
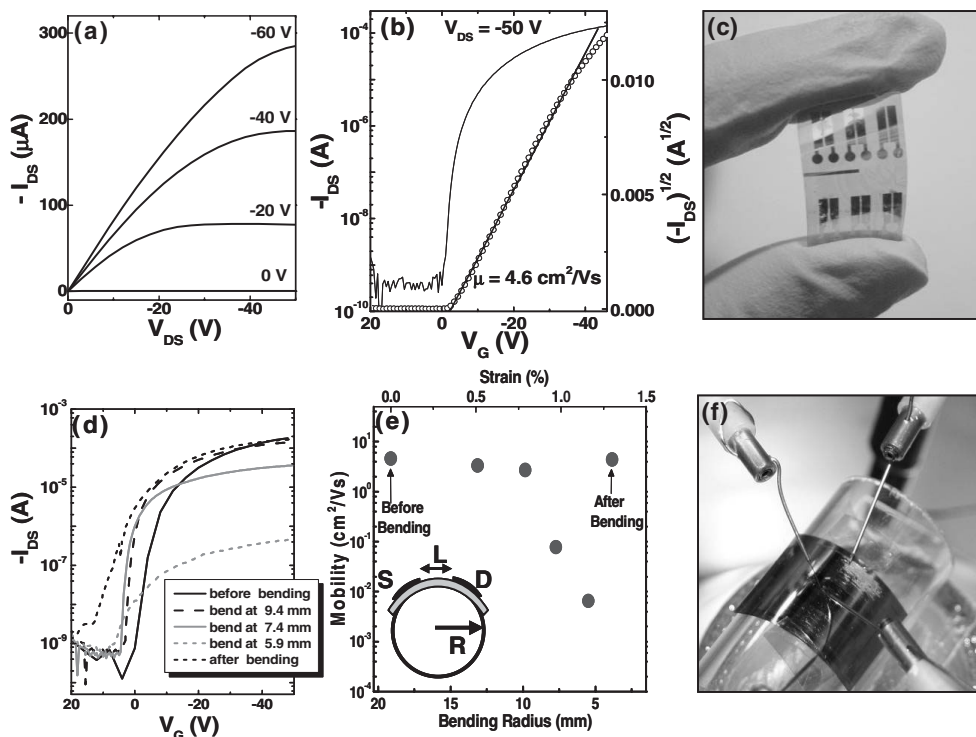
Figure 5. Organic single-crystal field-effect transistors on flexible substrates. a) The output and transfer characteristics of thin rubrene field-effect transistors fabricated from a flexible substrate. ($W = 978\ \mu m$, $L = 45\ \mu m$) b) Transfer and $I_{DS}^{1/2} - V_G$ curves. c) A digital photograph of a transparent, flexible, single-crystal rubrene transistor fabricated on an ITO–PET substrate. A close look reveals single crystals on the Au source–drain electrodes. d) An overlay of transfer curves ($V_{DS} = -50$ V) at different bending radii. Take note that the magnitude of the current is restored to nearly its original value after releasing the plastic substrate from a bend radius of 5.9 mm. e) The field-effect mobility as a function of bending radius (bottom axis) and strain (top axis). We caution that the "before bending" and "after bending" points should actually be plotted at infinity (planar geometry) and 0 % strain. We simply inserted these points for visualizing where the mobility lies relative to the mobilities of the bent substrates. All bending measurements were performed on substrates bent across the channel length as shown in the inset. f) A photograph of an experimental flexible single-crystal device as it is measured on a curved cylinder.

anisotropy effects and may deviate by a factor of two to five compared to reported values.[4–6,8] We also demonstrate the mechanical flexibility of single-crystal transistors by bending substrates to various radii as illustrated from the transfer curve overlays in Figure 5d. Figure 5d and e show the device field-effect mobility as a function of bending radius and strain. The flexible device can be bent to a radius of less than 1 cm (~ 9.4 mm; 0.74 % strain) without any significant loss in performance. The substrates were held in "bent" positions for approximately 1 h at each measured radius. These results are similar to those from a previous report;[17] however, when the substrate is bent from a radius of 7.4 to 5.9 mm, the mobility dramatically drops more than two orders of magnitude to 0.078 and 0.0065 cm^2 V^{-1} s^{-1}, respectively. Nevertheless, respective on/off ratios of approximately 10^5 and 10^3 are still observed at such strenuous bending. We did not conduct multiple bending cycles in this project. The acute bending induces a large interfacial strain on the crystal and possibly the dielectric, which results in a decrease of mobility. Interestingly, the mobility is restored to 91.3 % of the original value after releasing the flexible substrate from a bending radius of 5.9 mm (1.18 % strain) to the original "nonbent" position. The on/off ratio is also restored back to an original value of about 10^6.

These results evidently demonstrate the durability to flexing and imply that transistors fabricated from ultrathin single crystals may have potential use in applications where ruggedness and mechanical flexibility are a requirement. While our flexible transistors endure mild flexing, they are unlikely to be designed for severe treatment like those used in artificial skin applications where a bending radius of 2 mm has been successfully achieved.[12a,b]

In conclusion, we have demonstrated high-performance organic single-crystal transistors with electrical characteristics comparable to amorphous silicon and better than previously reported flexible organic thin-film transistors. Flexible transistors based on thin, conformable organic single crystals may give rise to alternative applications that can have a profound influence on consumer electronics.

Experimental

Crystal Growth: Rubrene single crystals were grown by a process similar to Kloc's method of horizontal physical vapor transport growth [13]. Slow growth, with a minimum of growth-nucleation sites on the inner walls of the glass cylinders are a suitable choice to produce large, thick crystals typically used in other reported studies [7]

with growth times of 6–24 h, and sublimation temperatures of about 280–300 °C. Typical flow rates used were 50 mL min^{-1}. However, rapid crystal growth results in very thin, large, and flat crystal flakes with a transparent appearance (20 min to 1 h growth time). For these results, an initial sublimation temperature of about 280–300 °C was again employed. At the moment nucleation was first observed on the inner glass cylinders, the temperature was increased to approximately 330 °C while a flow rate of about 100 mL min^{-1} was administered. It should be noted that specific parameters may vary from instrument to instrument, but the principle of rapid crystal growth remains the same. All crystals were grown in a flow of argon. Our growth apparatus did not use ultrahigh purity argon or any filter traps. We believe much higher mobilities can be obtained if extensive purification of the starting material is performed as well as utilizing high-purity gases and filters as other researchers have reported [10,11,13].

Device Fabrication: Single-crystal transistors were fabricated on conventional SiO$_2$ substrates containing a dielectric thickness of 300 nm on highly doped Si. A capacitance of 10 nF cm^{-2} was used to calculate hole mobility of a 300 nm SiO$_2$ dielectric while a capacitance of 1.9 nF cm^{-2} was used for a 1.5 μm thick PVP dielectric. For flexible transistors, a dielectric layer of PVP was spin-coated (~ 2000 rpm) on a 140 μm thick Kapton film or transparent ITO-coated (ITO: indium tin oxide) PET sheets. The dielectric solution was prepared from 22 wt % PVP (weight-average molecular weight, $M_w = 20\,000$), and 8 wt % poly(melamine-*co*-formaldehyde) methylated ($M_w = 511$) [22]. The substrates were baked at 100 °C for 10 min then at 200 °C for 10 min to provide crosslinking. Subthreshold slopes were multiplied by the capacitance of either SiO$_2$ or PVP for determining normalized subthreshold swings. The subthreshold slopes were calculated from the equation, $S = dV_G/d(\log I_{DS})$ [7]. The source–drain electrodes for flexible devices were evaporated from 5 nm Cr and 50 nm Au. The W/L values for our highest mobility devices were approximately 1.14 ($W = 400$ μm, $L = 350$ μm) for conventional "nonflexible" SiO$_2$ substrates and 21.73 ($W = 978$ μm, $L = 45$ μm) for flexible devices. The bending measurements were performed by attaching the flexible devices onto curved cylinders of different radii as shown in Figure 5e and f. We remark that device characteristics reported here are the 'best' in our measured devices. We also note that our devices did not deviate more than 10 % from repeated testing. More than 20 rubrene devices were tested in this study. Solutions of 10 mM NB (Aldrich) were prepared in dry toluene and conventional "nonflexible" substrates were allowed to soak for 1 h then rinsed with toluene followed by acetone and dried in a stream of N$_2$. Detailed results on flexible substrates with NB-modified electrodes were not reported because we found a large sample-to-sample variation in field-effect mobility. We believe the variation may be attributed to inefficient self-assembled monolayer adsorption from the rougher gold surface on the flexible substrates. The strain on devices can be calculated by the given equation:

$$\varepsilon = \left(\frac{d_f + d_s}{2R}\right)\frac{(1 + 2\eta + \chi\eta^2)}{(1 + \eta)(1 + \chi\eta)}$$

where ε is the strain, R is the bending radius, $\chi = Y_f/Y_s$ (Y_f, Y_s are the Young's moduli of the gate dielectric layer and substrate, respectively), and $\eta = d_f/d_s$ (d_f is the thickness of the gate dielectric layer and d_s is the thickness of the substrate) [23]. The thicknesses of the Kapton substrate and the PVP dielectric are 140 and 1.5 μm, respectively and $\chi \sim 1$. Here, the strain related to the above structure parameters is approximated to $d_s/2R$.

Instrumentation: SEM images were obtained with a JEOL JSM 6700F field-emission gun electron microscope. Samples were coated with approximately 5–10 nm of gold before imaging. Electrical characterizations were performed using a semiconductor parameter analyzer (HP 4155B). The film thicknesses for rubrene crystals were measured using a profilometer (Dektak 3030), an atomic force microscope (Digital Instruments), and the previously described SEM instrument.

[1] R. G. Kepler, P. E. Bierstedt, R. E. Merrifeld, *Phys. Rev. Lett.* **1960**, *5*, 503.

[2] M. Pope, E. Charles, C. E. Swenberg, *Electronic Processes in Organic Crystals and Polymers*, 2nd ed., Oxford University Press, Oxford **1999**, pp. 337–340.

[3] C. Goldmann, S. Haas, C. Krellner, K. P. Pernstich, D. J. Gundlach, B. Batlogg, *J. Appl. Phys.* **2004**, *96*, 2080.

[4] V. C. Sundar, J. Zaumseil, V. Podzorov, E. Menard, R. L. Willett, T. Someya, M. E. Gershenson, J. A. Rogers, *Science* **2004**, *303*, 1644.

[5] E. Menard, V. Podzorov, S.-H. Hur, A. Guar, M. E. Gershenson, J. A. Rogers, *Adv. Mater.* **2004**, *16*, 2097.

[6] V. Podzorov, E. Menard, A. Borissov, V. Kiryukhin, J. A. Rogers, M. E. Gershenson, *Phys. Rev. Lett.* **2004**, *93*, 086 602.

[7] V. Podzorov, S. E. Sysoev, E. Loginova, V. M. Pudalov, M. E. Gershenson, *Appl. Phys. Lett.* **2003**, *83*, 3504.

[8] R. Zeis, C. Besnard, T. Siegrist, C. Schlockermann, X. Chi, C. Kloc, *Chem. Mater.* **2006**, *18*, 244.

[9] H. Moon, R. Zeis, E.-J. Borkent, C. Besnard, A. J. Lovinger, T. Siegrist, C. Kloc, Z. Bao, *J. Am. Chem. Soc.* **2004**, *126*, 15 322.

[10] V. Y. Butko, X. Chi, D. V. Lang, A. P. Ramirez, *Appl. Phys. Lett.* **2003**, *83*, 4773.

[11] R. W. I. De Boer, M. E. Gershenson, A. F. Morpurgo, V. Podzorov, *Phys. Status Solidi A* **2004**, *201*, 1302.

[12] a) T. Someya, T. Sekitani, S. Iba, Y. Kato, H. Kawaguchi, T. Sakurai, *Proc. Natl. Acad. Sci. USA* **2004**, *27*, 9966. b) T. Someya, Y. Kato, T. Sekitani, S. Iba, Y. Noguchi, Y. Murase, H. Kawaguchi, T. Sakurai, *Proc. Natl. Acad. Sci. USA* **2005**, *35*, 12 321. c) U. Zschieschang, H. Klauk, M. Halik, G. Schmid, C. Dehm, *Adv. Mater.* **2003**, *15*, 1147. d) J. A. Rogers, Z. Bao, K. Baldwin, A. Dodabalapur, B. Crone, V. R. Raju, V. Kuck, H. Katz, K. Amundson, J. Ewing, P. Drzaic, *Proc. Natl. Acad. Sci. USA* **2001**, *98*, 4835.

[13] R. A. Laudise, C. Kloc, P. G. Simpkins, T. Siegrist, *J. Cryst. Growth* **1998**, *187*, 449.

[14] D. J. Gundlach, L. Jia, T. N. Jackson, *IEEE Electron Device Lett.* **2001**, *22*, 571.

[15] J. Takeya, C. Goldmann, S. Haas, K. P. Pernstich, B. Ketterer, B. Batlogg, *J. Appl. Phys.* **2003**, *94*, 5800.

[16] a) K. Nomura, H. Ohta, A. Takagi, T. Kamiya, M. Hirano, H. Hosono, *Nature* **2004**, *432*, 488. b) E. Menard, R. G. Nuzzo, J. A. Rogers, *Appl. Phys. Lett.* **2005**, *86*, 093 507. c) D.-Y. Khang, H. Jiang, Y. Huang, J. A. Rogers, *Science* **2006**, *311*, 208.

[17] G. H. Gelinck, H. E. A. Huitema, E. V. Veenedaal, E. Cantatore, L. Schrijnemakers, J. B. P. H. Van Der Putten, T. C. T. Geuns, M. Beenhakkers, J. B. Giesbers, B. H. Huisman, E. J. Meijer, E. M. Benito, F. J. Touwslager, A. W. Marsman, B. J. E. Van Rens, D. M. De Leeuw, *Nat. Mater.* **2004**, *3*, 106.

[18] Q. Cao, S.-H. Hur, Z.-T. Zhu, Y. G. Sun, C.-J. Wang, M. A. Meitl, M. Shim, J. A. Rogers, *Adv. Mater.* **2006**, *18*, 304.

[19] L. P. Ma, Y. Yang, *Appl. Phys. Lett.* **2004**, *85*, 5084.

[20] T. B. Singh, N. Marjanovic, G. J. Matt, S. Günes, N. S. Sariciftci, A. M. Ramil, A. Andreev, H. Sitter, R. Schwödiauer, S. Bauer, *Org. Electron.* **2005**, *6*, 105.

[21] G. Horowtiz, M. E. Hajlaoui, R. Hajlaoui, *J. Appl. Phys.* **2000**, *87*, 4456.

[22] F. C. Chen, C. W. Chu, J. He, Y. Yang, *Appl. Phys. Lett.* **2004**, *85*, 3295.

[23] a) Z. Suo, E. Y. Ma, H. Gleskova, S. Wagner, *Appl. Phys. Lett.* **1999**, *74*, 1177. b) H. Gleskova, S. Wagner, Z. Suo, *Appl. Phys. Lett.* **1999**, *75*, 3011.